Surface Science, **603** (2009) 1415-1426

Surface species studied by angle-resolved product desorption;

Emission mechanism and spatial distribution

Tatsuo Matsushima

Catalysis Research Center, Hokkaido University, Sapporo 001-0021, Japan

Corresponding author; T. Matsushima

tel: (+81)-29-874-1508

fax: (+81)-29-874-1508

e-mail:tatmatsu@mbr.nifty.com

Abstract

Recent progress and future developments in angle-resolved measurements of desorbing surface reaction products are reviewed for the analysis of surface species. Spatial and energy distributions of desorbing products with hyperthermal energy deliver the most direct structural information of the transition state including active intermediates and product formation sites. Knowledge of the desorption mechanism is requisite to achieve structural information since the method is directly linked to the chemical process. Structural analyses are exemplified in photoinduced O_2 desorption and CO oxidation, and compared with those from thermal N_2O decomposition and CO oxidation as well as their applications to steady-state catalytic processes.

Key words; Desorption dynamics, Angle resolved TPD, Surface chemical reaction, Nitrogen oxides, Carbon monoxide, Palladium, Platinum, Rhodium

1. Introduction

The configuration of transition state (TS) in gas-phase reactions is analyzed from the spatial and energy distributions of emitted products [1] or by femto-second spectroscopy during molecular

transformation [2], yielding the shape of the potential energy surface (PES). A similar approach to TS in surface reactions has been partly successful in limited cases and has been useful in the identification of active intermediates and reaction sites [3]. This paper is a review of such approaches to TS immediately before desorption in thermal and photoinduced processes. Information on both the desorption mechanism and energy partitioning is requisite for structural analysis since the method is directly linked to chemical processes; i.e., structural information depends on the product emission mechanism, which can be *dissociative* or *associative*.

TS in a surface reaction is still difficult to examine experimentally by means of fast surface spectroscopy because product molecules are quickly thermalized to the surface temperature before detection. In fact, the relaxation time of vibrationally excited molecules on metal surfaces is in the order of picoseconds [4]. Hence, density functional theory (DFT) with a generalized gradient approximation (GGA) has yielded many proposals for TS configuration without experimental examinations [5-7]. There is currently no way to determine the energy distributions of nascent products on metal surfaces. Only limited surface reactions, which emit product molecules with hyperthermal energy leading to collimated desorption, have been examined for the configuration analysis of TS from desorption dynamics [8-10].

Collimated *fragment* desorption from surface molecules has frequently been reported in electron-stimulated desorption ion angular distribution (ESDIAD), in which the emission is

initiated by the injection of electrons or photons [11,12]. The fragment desorption collimates mostly along the ruptured bond axis; thus, the resultant spatial distribution yields the structural information of parent molecules, i.e., their orientation. However, the collimation angle (providing the maximum flux) moves away from the bond axis direction when fragments are first emitted into surface-parallel ways as a result of the injection. This nascent fragment is called a hot atom for oxygen dissociation because of its high reactivity [13]. Thus, studies of such hot-atom-mediated desorption were not extended as ESDIAD work and were limited to only a few flat metal surfaces in which the hot atom does not desorb and, instead, the second species receiving the atom or its energy can leave the surface [13-16]. After detailed analysis of product desorption in ultra-violet photon-stimulated reactions of aligned O_2 on stepped Pt surfaces [17-20], it became clear that this hot-atom-mediated desorption exemplifies the typical relationship of the desorption mechanism toward the resultant spatial distributions of desorbing species, i.e., the structural information preserved in the distribution when the product is directly emitted from an associative process is different from that when a nascent fragment is first emitted parallel to the surface plane in a dissociative process [21]. In the former associative process, the collimation angle largely moves toward the local normal of the product formation site with increasing translational temperature [19]. This provides supplemental evidence for the collimation angle shift from the site normal observed in thermal CO oxidation [21]. In the latter

dissociative process, a simple momentum transfer mechanism is operative from the hot atom to the product leaving in an inclined way [17]. This mechanism has led to the first inclined fragment emission in the thermal dissociation of adsorbed molecules, in which the parallel momentum transfer is reproduced in a simpler way [22]. These close relationships suggest that a common principle is operative for inclined product emission in both thermal reactions and photo-induced reactions. Now we are at the point in which the experimental approach to the configuration of TS has begun in thermal surface reactions.

In this review, first, the spatial distributions of products in both photoinduced oxygen desorption and CO oxidation are discussed to yield information of TS or reaction sites, depending on the desorption mechanism. Then different structural information is shown from the similar angular distributions of desorbing N_2 and CO_2 in thermal reactions. In the next stage, both angle-resolved performance and state-resolved analysis must be combined, providing the configuration of TS through the desorption- and azimuth-angle dependences of the translational and internal energies. These dependences are requisite to get structural information of active surface species including reaction sites. Thus, product molecules must be analyzed both after angle-resolved procedures and before energy dissipation. Individual product molecules cannot provide surface structure information after desorption.

Unfortunately, no azimuth-angle dependence has been found in the flux of desorbing

hydrogen molecules in thermally activated $2H(a) \rightarrow H_2(g)$ on metal surfaces despite many attempts [23,24] and proposals [25]. In the energetics of this process, the structural information of reaction sites is missing [26,27]. Only four thermal desorption processes, $CO(a)+O(a) \rightarrow CO_2(g)$, $C(a)+O(a) \rightarrow CO(g)$, $2N(a) \rightarrow N_2(g)$, and $N_2O(a) \rightarrow N_2(g) + O(a)$, have so far shown remarkable desorption- and azimuth-angle dependences in either the flux or the energy of products [21,28,29].

2. Angle-resolved measurements

In ESDIAD, angle-resolved (AR) desorption measurements can be performed in a single ultra-high vacuum chamber. With the use of short laser pulses or electron beams, the signal due to fragments directly moving from the surface to the detector can be distinguished in time-resolved measurements because of the delayed arrival of fragments scattered by the chamber wall. This can be extended to AR translational and internal-energy measurements using a two-dimensional microchannel plate (MCP) detector [30].

On the other hand, in *thermal reactions*, at least three chambers must be combined because at least two slits should be operative between the sample surface and the analyzer, and high-speed pumping is requisite between the two slits [31]. The flux and both the translational

and internal energies of desorbing products must be analyzed after these AR procedures. The principle behind the apparatus is drawn in Fig. 1. The apparatus is an ultra-high vacuum system composed of a reaction chamber, a chopper housing and an analyzer, which are separately pumped. In the figure, a very large pumping rate can be established by a copper plate cooled to around 25 K. The reaction chamber has standard facilities for surface analysis, such as low-energy electron diffraction (LEED) and X-ray photoelectron spectroscopy optics and a quadruple mass spectrometer (QMS) [21]. The chopper house has a narrow slit facing the reaction chamber and contains a cross-correlation chopper blade for time-of-flight (TOF) measurements [32]. A sample crystal is rotated to adjust the desorption angle (θ; polar angle) and the crystal azimuth (ϕ) (Fig. 2). In this paper frequently describing the results on Pd(110) and Rh(110) surfaces, the azimuth angle (ϕ) is defined as a deviation from the [001] direction. Here, a new angle system is necessary to present the distribution in three-dimensional ways using the power functions of the cosine of the desorption angles (α,β) in the different planes. According to the rotation defining Eulerian angles, the relation between angles (α,β) and (θ,ϕ) is given by $\cos\theta = \cos\alpha \cos\beta$ and $\tan\phi = -\tan\beta / \sin\alpha$ [33]. For three-dimensional presentations, the experimental AR signals at definite (θ,ϕ) values are converted into the signal intensity at new coordinates (α,β) after smoothing the data points against varying θ values at fixed ϕ values [29].

For internal energy measurements after AR procedures, the optics for infrared (IR) chemiluminescence collection or the laser light for resonance-enhanced multi-photon ionization (REMPI) should be focused on the product flow after the second slit. The product density there is reduced to about 0.1% of that several mm from the surface [34,35]. Recently, Yamanaka constructed an apparatus for the IR emission detection of desorbing nascent product CO_2 using AR procedures. A meaningful signal was detected after the background emission was reduced to 0.05 % of that without cooled shielding around the optics [36].

3. Hot-atom-mediated desorption

In ESDIAD, the well-known principle that a fragment is emitted along the ruptured bond axis is available [37]. The fragment itself is directly emitted into the gas phase. Thus, the orientation of parent molecules is preserved in the spatial distribution of desorbing fragments [11,12]. This approach is acceptable when the emission is directly induced from the dissociation event and not collimated far from the surface normal. This kind of fragment emission has never been confirmed in thermal dissociations. In ESDIAD, on the other hand, the fragment emission closely parallel to the surface plane is obscured because the trajectory of desorbing ions is seriously affected by image forces or the ion itself is partially neutralized [11]. The parallel

emission becomes interesting in both hot-atom-mediated desorption and thermal dissociation, in which adsorbed molecules are likely to dissociate and the resultant fragments (or hot atoms) are first emitted parallel to the surface plane. Such ballistic movements of emitted fragments have frequently been confirmed by means of scanning tunneling microscopy (STM) [38,39].

No hot atom alone is desorbed into the gas phase. Instead, the molecules that receive momentum from the hot atom leave the surface. Such hot-atom-mediated desorption was examined in photoinduced emission of O_2 and CO_2 on stepped platinum surfaces as well as of O_2 on Ag(110) and noble gases on Pt(111) in the presence of O_2(a) [14-20]. On platinum surfaces, oxygen ad-molecules lie parallel to the surface plane and are likely to be localized on the terrace edge at small coverage because of the high adsorption energy. Thus, these molecules are oriented along the terrace edge, as confirmed by both STM and near-edge X-ray absorption fine-structure (NEXAFS) [40-42]. This O_2-covered stepped surface, such as Pt(112)=[(s)3(111)×(001) and Pt(113)(1×2)=[(s)3(111)×3(001)], provides a suitable stage for examining hot-atom-mediated desorption. These oxygen molecules are dissociated by ultraviolet light with a very small desorption cross section of about 3×10^{-19} cm^2 [20]. It yields a low quantum yield of 6×10^{-5}. This means that only about $1/10^4$ fraction of admolecules is dissociated at a usual photon flux of around 2×10^{15} photons/cm^2 per pulse, i.e., the dissociation event is surrounded by ad-molecules. The light is absorbed by the metal, exciting conduction electrons [16]. The

electron is trapped into definite anti-bonding states of O_2, leading to its dissociation. An emitted oxygen atom collides with neighbor O_2, leading to its desorption into the gas phase. The resultant spatial distribution of desorbed oxygen molecules is characteristic of the initial emission direction of hot atoms, i.e., the desorption is highly concentrated in the plane along the ruptured bond axis in an inclined way (Fig. 3) [20]. Here, a clean Pt(112) surface was exposed to $^{16}O_2$ at T_S = 100 K, and a non-polarized 193nm laser pulse with a fluence of about 2 mJ/cm^2 was introduced to the sample. The transient surface temperature increase was around 2 K only, yielding no thermal effect for the O_2 dissociation [43].

At small O_2 coverage, the O_2 desorption is collimated at around 15° off normal mostly in the plane along the terrace edge, whereas, at higher coverage, an additional component collimated at around 45° appears. The latter is due to a collision of the high energy hot atom with the nearest neighbor O_2, and the other is due to a collision with the next nearest neighbor O_2 [20]. The translational energy of the latter is around 1,700 K, much lower than that of the former, about 3,000 K. The leaving O_2 receives repulsive forces from the surface when its bond toward the metal atoms is broken, yielding inclined desorption. This desorption still has a memory of the orientation of parent molecules. Similar results were also observed on Pt(113)(1×2) [17]. At higher O_2 coverage, such desorption is obscured by overlapping with an enhanced desorption component collimated along the bulk surface normal.

4. Hot-atom-assisted reactive CO_2 desorption

The hot atom oxygen is reactive toward adsorbed CO, yielding CO_2. The product $^{13}C^{18}O^{16}O$ is detected with a similar quantum yield when the surface is covered by a mixture of $^{16}O_2$ and $^{13}C^{18}O$ [20]. Hereafter, ^{13}C and ^{18}O are simply referred to as C and O in the text. At small coverage, the product CO_2 desorption is again concentrated in the plane along the ruptured O_2 bond axis; i.e., the inclined CO_2 desorption is almost in the plane along the terrace edge (Figs. 4a and b). This inclined desorption involves two components collimated at 20° and 29° off normal in a similar way to O_2 desorption. The latter is extracted from the fast velocity component in the velocity distribution curve, showing a translational temperature of 6,200 K. The other one, collimating at 20°, shows a translational temperature of 2,650 K. These temperatures are due to the direct collision of hot atoms with adsorbed CO. The resultant CO_2 can receive high energy coming from the hot atom momentum and also the heat of CO_2 formation. On the other hand, at high coverage, another CO_2 desorption component becomes predominant, collimating along the local normal of the (111) terrace (Fig. 4c). This component is negligible at small coverage. This large component is due to the reaction on the terrace, which is also observed on flat Pt(111) at high coverage [13]. Its translational temperature reaches about

3,250 K. This component is due to only the heat of CO_2 formation; i.e., the hot atom momentum cannot be directly transferred into this CO_2. Its value is almost twice that of CO_2 formed in a thermally activated $CO(a)+O(a)\rightarrow CO_2(g)$ process. The reaction becomes possible, yielding high-energy CO_2, because the reactive oxygen atom enters the terrace highly covered by CO. The translational energy is enhanced on a highly covered surface [21]. Similar results were also observed on Pt(113)(1×2); i.e., at small coverage, the inclined CO_2 desorption appears in the plane along the terrace edge, whereas collimated CO_2 desorption at high coverage is along the local normal of both the (001) and (111) facets [18]. It should be noted that its collimation is in the local normal of (111) or (001) terraces. This supports the idea that the collimation angle shift from the site normal in thermal CO oxidation is due to the surface smoothing effect by conduction electrons [19]. The shift is caused by insufficient translational energy of product CO_2 and suppressed by high velocity product.

Thus, in both hot-atom-mediated and -assisted desorption, the orientation of O_2 molecules is preserved in the spatial distributions of desorbing O_2 and CO_2 in a different way from that in ESDIAD; i.e., it is almost preserved in a two-dimensional manner. This relationship between the orientation and the spatial distribution is useful to identify active species in thermal reactions as shown in the following sections. On the other hand, at high coverage, the trajectory of hot atoms does not affect the spatial distribution of the terrace component. It is merely controlled by the

shape of the terrace and the velocity. This shows the necessity to understand the desorption mechanism for the analysis of surface structures from the spatial distribution.

5. Fragment emission in thermal dissociation

In thermal dissociative (repulsive) desorption, the orientation of parent molecules is preserved in the spatial distribution of desorbing fragments in a similar manner to the above hot-atom-assisted desorption. In the thermal decomposition of adsorbed molecules, the released fragment has been believed to be quickly thermalized to the surface temperature before emission. Furthermore, the eventual desorption occurs mostly in an associative manner [44-46]. On the other hand, the recently reported inclined N_2 emission is exceptional [22]. It is due to direct emission from thermal N_2O decomposition on Pd(110), Rh(110), Ir(110), and Rh(100) [3]. This is the first example to show collimated fragment desorption in thermal decompositions on metal surfaces.

The N_2O decomposition is sensitive to surface structures [47]. On a (111) plane of Pt, Ir, Ni, Ag, and Rh, the desorption of adsorbed N_2O is completed below 120 K without dissociation. On the other hand, on an open (110) plane of Ni, Pd, Rh, and Ir, N_2O dissociates below 100 K. The reactivity of a (100) plane is between the above cases; i.e., N_2O dissociates on Rh(100) and

Ni(100) and not on Pd(100).

The inclined N_2 emission is observed in both the heating of N_2O-covered surfaces and its steady-state reduction at high temperatures [3]. A typical series of AR temperature-programmed desorption (TPD) spectra of desorbing N_2 during heating of N_2O-covered Rh(110) is reproduced at a small N_2O coverage in Fig. 5a [48]. Here, a clean rhodium (110) surface was exposed to N_2O at around 50 K, and, in the subsequent heating, N_2 desorption was monitored in an AR way. The spectrum shape is sensitive to the desorption angle. It shows five peaks at around 70 K (β_5-N_2), 95 K (β_4-N_2), 115 K (β_3-N_2), 140 K (β_2-N_2), and 160 K (β_1-N_2). β_1-N_2 yields a cosine distribution, indicating the desorption of adsorbed N_2, whereas the others commonly collimate at 69±3º off normal into the [001] direction (Fig. 5b-d). These are due to the decomposition of N_2O oriented in the [001] direction. The formation of each peak is modified by deposited oxygen because of the enhancement of adsorption energy [49]. The formation of β_5-N_2 and β_4-N_2 decreases quickly with increasing amounts of pre-adsorbed oxygen. On the other hand, that of β_3-N_2 and β_2-N_2 is maximized at around 6 % of the saturation oxygen level and completely suppressed above 15 %. This oxygen effect to the TPD spectrum was well simulated by means of the Monte-Carlo method [50,51].

The fragment N_2 emission is highly concentrated in the plane along the [001] direction. A three-dimensional distribution of desorbing N_2 was constructed in the steady-state N_2O+CO on

Pd(110) from its angular distributions in the plane along different crystal azimuths (Fig. 6a) [29]. This reduction is stable on Pd(110) in a wide temperature range (Fig. 7) [52], whereas it is highly retarded on Rh(110) when the N_2O pressure is higher than that of CO or H_2 [53]. Using the new polar angle system in Fig. 2(b), the resultant spatial distribution is well described as $\cos^{28}(\alpha \pm 45)\cos^{17}(\beta)$ at 520 K (Fig. 6). The distribution is very sharp against the crystal azimuth. This supports the idea that N_2O decomposes after being oriented along the [001] direction in the wide temperature range of 100-800 K.

6. Energy partitioning in adsorbed N_2O dissociation

Adsorbed N_2O was observed to be oriented along the [001] direction on Pd(110) by STM at 14 K [54] and by NEXAFS at 60 K [55]. The co-existing N_2O in an upright form bonding through the terminal nitrogen [56] is not reactive. According to DFT-GGA calculations by Kokaji, the nascent N_2 part, immediately after dissociation of the N-O bond, is attractive toward the nearest metal atom on Pd(110) and Rh(110) and repulsive toward the counter product oxygen [8,57,58]. Thus, the product N_2 has been proposed to be first emitted parallel to the surface plane and then scattered with deposited oxygen. This is not consistent with the results from AR-TPD, in which the N_2 emission is collimated around 45° on Pd(110) and 69° on Rh(110). The surface under

TPD conditions is not suitable for the observation of surface-parallel emission. For this examination, the surface should be free from both co-adsorbed oxygen and remaining N_2O. A suitable surface can be prepared in the steady-state reduction of N_2O under reducing conditions.

The surface-parallel N_2 emission can be observed on Rh(110) at around 300 K when deposited oxygen is removed by hydrogen [53]. The N_2 emission is collimated at around 80° off normal, which is almost a limiting value estimated from the van der Waals' radius of N_2 [59]. The parallel emission is not disturbed by adsorbed hydrogen atoms. In the steady-state N_2O+CO reaction, however, it is difficult to confirm this parallel emission. The collimation angle in this steady-state reduction on Rh(110) shifts from 65° off normal towards 45° with decreasing surface temperature in the range of 530-450 K. This shift is due to increasing amounts of adsorbed CO because the collimation angle becomes insensitive to the surface temperature above 530 K [59]. Below 450 K, no steady-state reduction proceeds because the surface is highly covered by CO, more than half a monolayer. Upright CO(a) retards the N_2O adsorption and also shifts the collimation angle of N_2 emission. The latter effect is due to the scattering of nascent N_2 moving parallel to the surface plane because of the large scattering cross section of standing CO [60-62]. In the experiments, the fraction of N_2 signal due to the cosine distribution is enhanced at high CO pressures. The split angular distribution suggests the presence of at least two desorption components with different collimation angles [53,59]. Adsorbed CO suppresses

the component that is closely surface-parallel. The remaining component is collimated at around 45°. Only the component collimated at 40-50° is observed on Pd(110). It is insensitive to the presence of adsorbed CO. Thus, there must be another mechanism to yield the collimation angle around 45° regardless of the adsorbed CO.

The N_2 desorption is highly concentrated in the plane along the ruptured bond axis. On Pd(110), the N_2 emission is sharply distributed in a narrow range of the azimuth angle (Fig. 6). In order to leave the surface with a collimation angle of around 45°, the nascent product must receive repulsive forces from metal atoms as well as the repulsive force exerted from the counter-product oxygen. In the former repulsion, the force must be induced from either the translational or the rotational mode. According to Kokaji's molecular dynamics (MD) simulations, the rotational motion in the nascent N_2 is highly excited in a cartwheel form because the adsorbed N_2O is bent and the nascent fragment will receive strong torque [8]. In the subsequent energy partition, the rotational energy might be used to enhance the momentum along the surface normal. Here, the rotational energy around the collimation angle would be interesting to understand this partitioning mechanism. The rotation energy distribution of N_2 can be analyzed by REMPI but has not been analyzed after AR procedures [34]. The rotational energy of desorbing O_2 in the hot-atom-mediated desorption is also interesting because there is a close similarity in the inclined desorption between the photo-desorbed O_2 and the N_2 in the N_2O

decomposition.

7. N_2 emission in NO reduction

Nitrous oxide was proposed to be an intermediate in NO reduction on rhodium surfaces already in 1978 [63]. This metal yields the best catalytic activity for deNOx treatments probably because NO is dissociated on open Rh surfaces even at around room temperature and the resultant surface nitrogen and oxygen are reactive enough to be quickly removed by simple reagents. At high temperatures, the surface-nitrogen removal proceeds as $2N(a) \rightarrow N_2(g)$ (β-N_2 -formation). On the other hand, at temperatures below 500-700 K, the δ-N_2 formation of $N(a)+NO(a) \rightarrow N_2O(a) \rightarrow N_2(g)+O(a)$ was suggested to contribute to the N_2 emission [64]. In fact, N_2O is frequently found in NO reduction over metal catalysts [65]. Nevertheless, N_2O formation has been treated as a side reaction probably because it is inert on flat or oxygen-covered metal surfaces [66]. Furthermore, it has been difficult to find direct evidence of the participation of this species toward N_2 formation because of the absence of spectroscopic evidence of adsorbed N_2O in the course of catalyzed NO reduction [67,68]. This is not surprising because of the small heat of adsorption of N_2O, about 29 kJ/mol. The surface residence time of this species is estimated to be shorter than nanoseconds above 400 K suitable for the steady NO reduction.

Even at high pressures, its observation is obscured by the presence of reactants NO(a) and CO(a), for example. In addition, vibrational spectroscopy is probably insensitive toward surface-parallel forms of adsorbed N_2O [56]. AR product desorption measurements in steady-state NO reduction, however, show the inclined N_2 desorption characterizing the N_2O decomposition under limited conditions, as described in the following sections. This is not unreasonable because adsorbed N_2O can be oriented in a suitable way before dissociation even at 800 K, as seen in Fig. 7. A surface residence time of approximately the nanosecond order is long enough to be oriented along the [001] direction. Structure-sensitive desorption dynamics provides the most direct method to identify shortly trapped active intermediates.

The inclined N_2 emission was first found in TPD work of NO-covered Pd(110) by Ikai and Tanaka [69,70]. They also confirmed, by means of an isotope tracer, that this inclined N_2 comes from the reaction of adsorbed NO with an adsorbed nitrogen atom; i.e., ^{15}N atoms were first deposited on Pd(110) and further exposed to ^{14}NO, and in the subsequent heating, desorbing nitrogen was analyzed in an AR way. $^{14}N^{15}N$ is desorbed into an inclined way, and $^{15}N_2$ is emitted along the surface normal.

In the NO reduction on Pd(110), Rh(110), and Rh(100) surfaces, at least three surface-nitrogen removal pathways are operative. The β-N_2 formation pathway, $NO(a) \rightarrow N(a)+O(a)$ and $2N(a) \rightarrow N_2(g)$, is operative at temperatures above 750 K on Rh(100), as shown in

Fig. 8. The kinetics of this process has been well characterized on this surface, showing a high activation energy [71,72]. The reaction rate increases steeply at around 800 K and emits N_2 along the surface normal. These findings agree well with the kinetics of β-N_2 formation. On the other hand, the reaction shows a small activation energy in the range of 500-800 K. The product N_2 is mostly emitted into an inclined way in the plane along either the [001] or [010] direction. The collimation angle is close to 70°, showing N_2O decomposition. This collimation of desorbing N_2 is also observed in AR-TPD of N_2O-covered Rh(100) surfaces [73]. The N_2 formation from NO(a)+N(a) has been kinetically speculated to be below about 750 K [71]. The spatial distribution work shows clearly that the reaction passes through the intermediate N_2O(a). A similar pathway shift with increasing surface temperature was derived on Rh(110) and Pd(110), where the δ-N_2 formation pathway highly contributes below 500 K [52,74]. Thus, only angle-resolved desorption measurements under steady-state conditions will separate the three pathways of surface-nitrogen removal, i.e., the formation of β-N_2 and δ-N_2 and the N_2O desorption.

8. Associative desorption and energy partitioning

In the above dissociative desorption, the momentum initially given on either the hot atom or the

emitted fragment is preserved in the spatial distribution of desorbing products although it is only in a two-dimensional way. Nevertheless, the orientation of parent molecules is derived, yielding information that is useful to identify active intermediates with a short surface residence time. On the other hand, in a thermally activated *associative* desorption, such as $2H(a) \rightarrow H_2(g)$, $2N(a) \rightarrow N_2(g)$, $C(a)+O(a) \rightarrow CO(g)$, $CO(a)+O(a) \rightarrow CO_2(g)$, and $CH_3(a)+H(a) \rightarrow CH_4(g)$, the product emission is, to some extent, sharply collimated along the surface normal on limited flat surfaces [21,75]. There is no breaking bond to control the direction of repulsive forces operative to leaving products. The repulsive force is exerted from the reaction site because of the close contact of nascent bulky products. The collimation angle is mostly controlled by the shape of the reaction site.

Here, it is noteworthy that the mechanism exerted by the repulsive force from the surface site is highly converted into the translational mode. In fact, the translational energy of desorbing molecules is usually maximized at the surface normal on a flat surface or remains constant with increasing shift from the surface normal [75]. On the other hand, the well-known Van Willigen's model predicts that the translational energy steeply increases with increasing desorption angle. In this model, the repulsive potential energy surface is assumed to be flat along the surface plane and only the translational mode is considered [76]. The kinetic energy should increase steeply with an increase in the desorption angle, since only the velocity component

perpendicular to the surface plane is enhanced by a constant amount even at large desorption angles. In fact, both the rotational and vibrational modes are to some extent excited in desorbing products H_2, N_2, and CO_2 in associative desorption [34]. Recently, Yamanaka succeeded in achieving infrared chemi-luminescence from the product CO_2 in CO oxidation on Pd(111) and Pd(110) after AR procedures [9,10]. With increasing desorption angle, the obtained rotational energy on Pd(111) increases steeply, and the vibrational energy decreases slowly.

In the CO oxidation on Pd(111), the product CO_2 molecule desorbing along the surface normal shows a high translational temperature, about 2,300 K at T_S= 700 K [21], and a lower rotational temperature, about half of the surface temperature (Fig. 9). At large desorption angles, the translational temperature is close to the surface value, and the rotational one is about twice the surface temperature even at 30°. In marked contrast to Willigen's assumptions, these observations indicate the occurrence of energy partitioning into either the translation or rotation modes in the repulsive desorption event. The repulsive forces operative to the product are efficiently converted into the translational form along the surface normal, whereas they are more efficiently converted into the rotational modes in the molecules desorbing at large desorption angles. The repulsive force is due to Pauli repulsion, since no chemical bond is formed from CO_2 to surface palladium atoms. This repulsion decreases steeply with increasing distance from the surface, as expected from the repulsive part in Lennard-Jones potential [77]. In such a highly

decreasing force field, the leaving molecule receives torque in a desorption event when it is inclined against the surface plane (Fig. 9d) [78]. The resultant desorbing molecule will have a small translational energy, yielding a broad angular distribution. On the other hand, the repulsive force is efficiently converted into the translational mode when the transition state is upright or parallel to the surface plane, and the angular distribution becomes sharp. On Pd(111), the transition state of CO_2 partly involves inclined components that may be induced by either restricted translations or bending motions.

The inclination of the transition state may depend on the crystal azimuth over an anisotropic surface. Thus, this azimuth dependence will appear in the rotational energy. In fact, Yamanaka has succeeded in observing such anisotropy in desorbing CO_2 in the CO oxidation on Pd(110) [9,10]. On Pd(110)(1×1), the rotational temperature in the normal direction, which reaches around 950 K at the surface temperature of 700 K, decreases quickly with increasing shift from the surface normal in the plane along the [001] direction, whereas it is fairly constant in the plane perpendicular to it; i.e., the rotational mode is excited in CO_2 molecules desorbing into the plane along the$[1\bar{1}0]$ direction. A remarkable anisotropy was already observed in the translational modes of desorbing CO_2 on this surface; i.e., the conversion into the translational motion is more efficient in the plane along the $[1\bar{1}0]$ direction than in that perpendicular to it (along the [001] direction). The mechanism for this predominance was once proposed to be due

to the surface corrugation; i.e., the motion of the transition state CO_2 along the [001] direction is more hindered by large corrugations or easier along the [$1\bar{1}0$] direction because of the smooth close-packed arrangements. The above remarkable anisotropy of rotational energy shows a significant contribution of the energy partitioning effect. The CO_2 molecule in the transition state is suggested to be inclined in the plane along the [$1\bar{1}0$] direction [9,10]. The anisotropy in the rotational energy is different when the surface is reconstructed. This work shows again the importance of AR-internal energy measurements to approach the configuration of TS.

9. Normally directed desorption and reaction-site shape

The energy partitioning in associative (repulsive) desorption gives a base to approach the shape of the reaction site being preserved in sharply collimated product emission. On flat surfaces, such as Pd(111), Pt(111), Rh(111), and Pd(100), the product CO_2 desorption is sharply collimated along the surface normal [21]. The distribution is symmetric about the surface normal axis on Pd(100) and Pd(111). No structural information can be derived from such symmetric distributions. On non-reconstructed (110)(1×1) of Pd, Rh, Pt, and Ir, which shows remarkable anisotropy, CO_2 desorption is collimated along the surface normal, and its distribution depends on the crystal azimuth [21]. It is sharp in the plane along the [001]

direction and broad in the plane perpendicular to it. When the surface has inclined facets wider than two-atom spacing, such as Pt(110)(1×2)=[(s)3(111)×3($\bar{1}$ $\bar{1}$ 1)], Pt(113)(1×2)=[(s)3(111)×3(001)], Pt(112)= [(s)3(111)× (001)], and Pt(335)= [(s)4(111)×(001)], CO_2 desorption is collimated off normal, closely along the local normal of the facets with a (111) structure (Fig. 10). Facets with two-atom spacing are not wide enough to emit the product CO_2 in an inclined way, as seen on Pd(110)(1×1), probably because a hollow site suitable for oxygen adsorption is not far from the nearest inclined facets. Mobile CO ad-molecules can visit oxygen atoms in a wide area and react with more active oxygen. Thus, CO_2 is formed on either the oxygen adsorption site or nearby even if its activation shifts the adsorption position to some extent [79].

This selection of reactive oxygen can be applied to identify CO_2 formation sites in the course of the catalyzed reaction. In the steady-state CO oxidation on Pt(113)(1×2), the product from (111) facets can be separately analyzed from that on (001) facets since CO_2 desorption from the former facets collimates at about 25° off normal whereas that from the latter collimates at about -25° in an opposite direction. At low CO pressures (P_{CO}<<P_{O2}) in the steady-state CO oxidation, where O(a)>>CO(a), CO_2 desorption mostly collimates along the local normal of (111) facets. On the other hand, its desorption shifts primarily along the (001) facet normal when the CO pressure is close to the kinetic transition point or above it, where CO(a)>>O(a).

The remaining oxygen is localized on the [001] facets. This is reasonable because of the higher reactivity of oxygen on (111) terraces toward adsorbed CO. The binding energy of oxygen on (111) facets is smaller than that on (001) facets. The oxygen on (001) facets can react with CO after most of the oxygen is consumed on (111) parts since mobile CO(a) can visit many oxygen adatoms before reaction.

The distribution of desorbing CO_2 varies when the surface structure changes. For example, reconstructed Pt(110)(1×2) having three-atom wide terraces is converted into non-reconstructed (1×1) when the CO pressure exceeds a critical kinetic value at which the rate-determining step is switched from CO adsorption to oxygen dissociation. Above the critical pressure, CO is accumulated to the level equilibrium to the CO partial pressure. Concomitantly, the CO_2 desorption shifts from the two-directional distribution into the normally directed one whenever the CO coverage reaches half a monolayer or above (Fig. 11). In the former, the CO_2 desorption is collimated at about ±26° off normal, closely along the local normal of the (111) facet. It is interesting to see the two-directional desorption even above the critical point when the CO coverage is below half a monolayer. The remaining (1×2) reconstructed part still plays the main role in producing CO_2, suggesting a high potential of reaction sites on inclined (111) facets [80].

10. Future developments

In the studies of the above-described associative CO_2 or dissociative N_2 desorption, the distributions of the flux and translational energy of desorbing products have been exemplified to provide structural information about its reaction site, i.e., its shape for associative desorption, as well as the orientation of parent molecules for dissociative reactions. The resultant desorption dynamics provides the most direct site-identification method applicable in the course of catalyzed reactions. The information is still available even if the product emission is not rate-determining because desorption dynamics is not affected by processes occurring before product formation.

The application of AR product desorption analysis to surface-structural information is still restricted to a few thermal reactions and has a limited extent. Such an analysis will deliver more information when it can be performed at a state-selective level. In fact, the present situation of surface reaction dynamics that is far from that of gas phase reactions is due to the absence of internal energy data of desorbing products in AR ways. In particular, knowledge on the role of vibrational excitation is missing, even though the vibration may be excited before the desorption event. In both surface- and gas-phase reactions, product molecules with hyper-thermal energy are emitted into three-dimensional space, showing translational and internal energies that are sensitive to emitted directions. Such angle dependence is still missing, even in desorbing

hydrogen molecules, from the associative desorption of hydrogen adatoms on metal surfaces [25,26,34,]. Their internal energies have been analyzed in non-AR ways (see Fig. 1). Such averaged measurements have an obscured dynamic approach to surface reaction sites. The state-selective analysis of desorbing products should be combined with angle-resolved performance; for example, REMPI techniques should be applied to products after AR procedures. This combination is more promising than IR chemi-luminescence, in which state-resolved analysis is difficult with high resolution [36]. This next-generation analysis becomes important to improve the AR-desorption method because each energy state of desorbing products will show different structural information.

The relationship of desorption dynamics to site structures will be elaborated by adding the desorption-angle dependence of the internal energies. This dependence will show the mechanism of energy partitioning into the rotational, vibrational, and translational modes in a repulsive desorption event. Furthermore, it will deliver the configuration of transition states immediately before desorption when the angle dependence varies with the crystal azimuth. This correlation has been characterized neither experimentally nor theoretically because of the absence of desorption-angle dependence of each energy state population.

If a theoretical approach is taken, use of the *detailed balanced principle* for adsorption-desorption processes should not be assumed without confirming its applicability. A

desorption process is not necessarily the reverse of adsorption. Desorbing molecules hold surface-structural information. Desorption dynamics must involve surface-structural descriptions. Fortunately, no azimuth dependence has been found in the flux and energy of desorbing product hydrogen molecules, and no catastrophe has yet occurred in their desorption dynamics [7].

Furthermore, little is known about energy transfer between surfaces and desorbing molecules. Electronic excitations have been confirmed in the bonding of chemical species to metal surfaces. The adsorption energy is not directly transferred into phonon modes [81-83]. Similar situations may be expected for breaking of chemical adsorption bonds, although such an event has not been observed yet. In the future, energy distributions of nascent product molecules will hopefully be analyzed before desorption. This development, which will revolutionize surface reaction dynamics, is not impossible in principle, since vibration frequency is much shorter than energy relaxation.

References

[1] P. Casavecchia, N. Balucani and G. G. Volpi, Annu. Rev. Phys. Chem. 50 (1999) 347.

[2] J.C. Polanyi and A.H. Zewail, Acc. Chem. Res. 28 (1995) 119.

[3] T. Matsushima, Prog. Surf. Sci. 82 (2007) 435.

[4] H. Ueba, Prog. Surf. Sci. 55 (1997) 115.

[5] A. Gross, Surf. Sci. Rep. 32 (1998) 291.

[6] A. Gross, Surf. Sci. 500 (2002) 347.

[7] W. Brenig, E. Pehlke, Prog. Surf. Sci. 83 (2008) 263.

[8] I. Kobal, A. Kokalj, H. Horino, Y. Ohno and T. Matsushima, Trends in Chem. Phys. 10 (2002) 139.

[9] T. Yamanaka and T. Matsushima, Phys. Rev. Lett. 100 (2008) 026104.

[10] T. Yamanaka, Phys. Chem. Chem. Phys. 10 (2008) 1.

[11] R. H. Stulen, Prog. Surf. Sci. 32 (1989) 1.

[12] R.D. Ramsier and J.T. Yates, Jr., Surf. Sci. Rep. 12 (1991) 243.

[13] W.D. Mieher and W. Ho, J. Chem. Phys. 91 (1989) 2755.

[14] Q.-S. Xin and X.-Y. Zhu, Surf. Sci. 347 (1996) 346.

[15] A.N. Artsyukhovich and I. Harrison, Surf. Sci. 350 (1996) L199.

[16] S.R. Hatch, X.-Y. Zhu, J.M. White and A. Campion, J. Phys. Chem. 95 (1991) 1759.

[17] M. Sano, Y. Ohno, T. Yamanaka, T. Matsushima, E.B. Quinay and K. Jacobi, J. Chem. Phys. 108 (1998) 10231.

[18] T. Yamanaka, Y. Inoue and T. Matsushima, J. Chem. Phys. 110 (1999) 2597.

[19] S. Han and T. Matsushima, Phys . Chem. Chem. Phys .7 (2005) 651.

[20] S. Han, Y. Ma and T. Matsushima, J. Chem. Phys. 123 (2005) 94702.

[21] T. Matsushima, Surf Sci. Rep. 51 (2003) 1.

[22] Y. Ohno, K. Kimura, M. Bi and T. Matsushima, J. Chem. Phys. 110 (1999) 8221.

[23] M. Balooch, M.J. Cardillo, D.R. Miller and R.E. Stickney, Surf. Sci. 46 (1974) 358.

[24] H.P. Steinrück, A. Winkler and K.D. Rendulic, Surf. Sci. 152/153 (1985) 323.

[25] D. Wetzig, M. Rutkowski and H. Zacharias, Phys. Stat. Sol. (A) 159 (1997) 263.

[26] H. A. Michelsen and D. J. Auerbach, J. Chem. Phys. 94(1991) 7502. Cu(111)

[27] C.T. Rettner, H.A. Michelsen and D.J. Auerbach, J. Chem. Phys. 102 (1995) 4625.

[28] A. V. Walker and D. A. King, J. Chem. Phys. 112 (2000) 1937.

[29] Y. Ma, T. Matsushima, K. Shobatake and A. Kokalj, J. Chem. Phys. 124 (2006) 144711.

[30] M. Wilde, K. Fukutani, Y. Murata, M. Kampling, K. Al-Shamery and H. J. Freund, Surf. Sci. 427/428 (1999) 27.

[31] M. Kobayashi and Y. Tuzi, J. Vac. Sci. Technol. 16 (1979) 685.

[32] G. Comsa, R. David and B. J. Schumacher, Rev. Sci. Instrum. 52 (1981) 789.

[33] H. Goldstein; *Classical Mechanics*, 2nd Ed. (Addison-Wesley, Reading, Mas. 1980) p. 143.

[34] A. Hodgson, Prog. Surf. Sci. 63 (2000) 1.

[35] H. Uetsuka, K. Watanabe and K. Kunimori, Surf. Sci. 363 (1996) 73.

[36] T. Yamanaka and T. Matsushima, Rev. Sci. Inst. 78 (2007) 034105.

[37] T. E. Madey, D. E. Ramaker and R. Stockbauer, Ann. Rev. Phys. Chem. 35 (1984) 215.

[38] J. Wintterlin, R. Schuster and G. Ertl, Phys. Rev. Lett. 77 (1996) 123.

[39] B. C. Stipe, M. A. Rezaei and W. Ho, J. Chem. Phys. 107 (1997) 6443.

[40] W. Ho, Acc. Chem. Res. 31 (1998) 567.

[41] T. Yamanaka, T. Matsushima, S. Tanaka and M. Kamada, Surf. Surf. 349 (1996) 119.

[42] S. Wako, M. Sano, Y. Ohno, T. Matsushima, S. Tanaka and M. Kamada, Surf. Sci. 461 (2000) L537.

[43] S.S. Mann, B.D. Todd, J.T. Stuckless, T. Seto and D.A. King, Chem. Phys. Lett. 183 (1991) 529.

[44] D.-H. Kang and M. Trenary, Surf. Sci. 519 (2002) 40.

[45] E. Demirci, J. Stettner, M. Kratzer, R. Schennach and A. Winkler, J. Chem. Phys. 126 (2007) 164710._

[46] H.H. Sawin, R.P. Merrill, J. Chem. Phys. 73 (1980) 996.

[47] A. V. Zeigarnik, Kinet. & Catal. 44 (2003) 233.

[48] K. Imamura, H. Horino, I. Rzeznicka, I. Kobal, A. Kokalj, Y. Ohno, B. E. Nieuwenhuys, A. Hiratsuka, T. Matsushima, Surf. Sci. 566/568 (2004) 1076.

[49] H.H. Huang. C.S. Seet, Z. Zou and G.Q. Xu, Surf. Sci. 356 (1996) 181.

[50] V.P. Zhdanov and T. Matsushima, Surf. Sci. 601 (2007) 2373.

[51] V. P. Zhdanov and T. Matsushima, Surf. Sci. 583 (2005) 253

[52] Y.-S. Ma and T. Matsushima, Catal. Today, 111 (2006) 302.

[53] T. Matsushima, Phys. Chem. Chem. Phys. 9 (2007) 3031.

[54] K. Watanabe, A. Kokalj, Y. Inokuchi, I. I. Rzeznicka, K. Ohshimo, N. Nishi and T. Matsushima, Chem. Phys. Lett. 406 (2005) 474.

[55] K. Watanabe, A. Kokalj, H. Horino, I. I. Rzeznicka, T. Takahashi, N. Nishi and T. Matsushima, Jpn. J. Appl. Phys. Part 1, 45 (3B) (2006) 2290.

[56] S. Haq and A. Hodgson, Surf. Sci. 463 (2000) 1.

[57] A. Kokalj, I. Kobal and T. Matsushima, J. Phys. Chem. B 107 (2003) 2741.

[58] A. Kokalj and T. Matsushima, J. Chem. Phys. 122 (2005) 34708.

[59] T. Matsushima, O. Nakagoe, K. Shobatake and A. Kokalj, J. Chem. Phys. 125 (2006) 133402.

[60] B. Poelsema, R. L. Palmer and G. Comsa, Surf. Sci. 123 (1982) 152.

[61] G. Parschau and K. H. Rieder, Surf. Sci. 257(1991) L628.

[62] K. A. Peterlinz, T. J. Curtiss and S. J. Sibener, J. Chem. Phys. 95 (1991) 6972

[63] C. T. Campbell and J. M. White, Appl. Surf. Sci. 1 (1978) 347.

[64] T.W. Root, L.D. Schmidt and G.B. Fisher, Surf. Sci. 134 (1983) 30.

[65] G. Centi, G. E. Arena and S. Perathoner, J. Catal. 216 (2002) 443.

[66] V. P. Zhdanov and B. Kasemo, Surf. Sci. Rep. 29 (1997) 31.

[67] E. Ozensoy, C. Hess and D.W. Goodman, J. Am. Chem. Soc. 124 (2002) 8524.

[68] E. Ozensoy and D.W. Goodman, Phys. Chem. Chem. Phys. 6 (2004) 3765.

[69] M. Ikai, H. He, C.E. Borroni-Bird, H. Hirano and Ken-ichi Tanaka, Surf. Sci. Lett. 315 (1994) L973.

[70] M. Ikai and Ken-ichi Tanaka, J. Phys. Chem. B 103 (1999) 8277.

[71] Se H. Oh, G.B. Fisher, J.E. Carpenter and D W. Goodman, J. Catal. 100 (1986) 360.

[72] M.J.P. Hopstaken and J.W. Niemantsverdriet, J. Phys. Chem. B, 104 (2000) 3058.

[73] T. Matsushima, J. Phys. Chem. C 111 (2007) 6422. .

[74] I. I. Rzeznicka, Y.-S. Ma, G. Cao and T. Matsushima, J. Phys. Chem. B, 108 (2004) 14232.

[75] G. Comsa and R. David, Surf. Sci. Rep. 5 (1985) 145.

[76] W. van Willigen, Phys. Lett. 28A (1968) 80.

[77] P.W. Atkins; in "*The Elements of Physical Chemistry*", 2nd Ed., (Oxford Univ. Press., 1996) Chapter 10.

[78] G. W. Coulston and G. L. Haller, J. Chem. Phys. 95 (1991) 6932.

[79] A. Alavi, P. Hu, T. Deutsch, P. L. Silvestrelli and J. Hutter, Phys. Rev. Lett. 80 (1998) 3650.

[80] I.I. Rzeznicka, M.G. Moula, L.M. Garza, Y. Ohno and T. Matsushima, J. Chem. Phys. 119 (2003) 9829.

[81] H. Nienhaus, Surf. Sci. Rep. 45 (2002) 1.

[82] E. Hasselbrink, Curr. Opin. Solid State Mater. Sci. 10 (2007) 192

[83] A. M. Wodtke, D. Matsiev and D. J. Auerbach, Prog. Surf. Sci. 83 (2008) 167.

(Figure Captions)

Fig. 1 The principle behind the apparatus of angle-resolved product desorption measurements incorporating time-of-flight techniques. The reaction chamber is an ordinary UHV apparatus with standard facilities for surface analysis and a mass spectrometer. Either the chopper house or the reaction chamber must be evacuated with a large pumping rate. A sample crystal holding is inserted as well as the size of the first slit (S1). The analyzer can not detect the crystal surface behind gold rods at a desorption angle of 90°. A pseudo-random chopper blade for cross-correlation time-of-flight techniques is drawn.

Fig. 2 (a) Crystal azimuth ϕ and desorption angle θ used in the experiments for Pd(110). (b) New polar angle system (α,β) in the data analyses for Pd(110). The plane at a fixed α value is shown as crosshatched.

Fig. 3 Angular distributions of oxygen desorbed by 193-nm irradiation in the plane along the surface trough on Pt(112). (a) 0.05-monolayer (ML) O_2, (b) 0.1-ML O_2, (c) 0.3-ML O_2. The signal on the ordinate was normalized to that in the normal direction in (c). Typical deconvolutions are shown by broken curves. A side view of Pt(112) along the surface trough, a

collision mechanism, and the polar angle (θ_b) along the trough are shown on the top.(Ref. 20)

Fig. 4 (a) Angular distributions of desorbing $^{13}C^{18}O^{16}O$ by 193 nm irradiation on Pt(112) at 0.05-ML$^{16}O_2$+0.09-ML$^{13}C^{18}O$ in the normally directed plane along the trough. The fastest component derived from the velocity distribution is shown by closed triangles. The remaining fast component is drawn by broken curves. The solid line stands for their summation. The open circles show the observed total flux. A side view of Pt(112) along the surface trough and a collision-inducing oxidation mechanism are shown on the top. (b) and (c); Angular distribution of $^{13}C^{16}O^{18}O$ in the plane perpendicular to the trough. $^{16}O_2$ was first dosed to 0.05 ML or 0.3 ML and then 0.09-ML $^{13}C^{18}O$ was adsorbed. Typical deconvolutions are drawn by broken curves. θ_a is the polar angle perpendicular to the trough. A side view of the terrace sites is shown on the top. (Ref. 20)

Fig. 5 (a) AR-TPD spectra of $^{15}N_2$ from Rh(110) exposed to 0.15 ML $^{15}N_2O$ at 50-55 K. The signal was corrected by subtraction of the $^{15}N_2O$ fragmentation. The curves were deconvoluted into five Gaussian peaks. Angular distributions of desorbing $^{15}N_2$ in the plane along the [001] direction, (b) β_1-N_2, (c) β_4-N_2 and (d) β_5-N_2. A top view of Rh(110) is shown on the top. (Ref. 48)

Fig. 6 Angular distributions of desorbing N_2 at different crystal azimuths (ϕ =0°, 25°, and 40°) in the steady-state N_2O reduction on Pd(110) at $P_{N2O} = 4.4\times10^{-4}$ Pa, $P_{CO} = 0.7\times10^{-4}$ Pa, and T_S = 520 K. The signal was plotted in a common scale. The solid curves are simulated by the inserted equations. The resultant N_2 distribution on 3-D coordinates is inserted as well as the best fitted equation. (Ref. 30)

Fig. 7 (a) Temperature dependence of $^{15}N_2$ and $^{13}CO_2$ signals at their collimation angles in a steady-state $^{15}N_2O$ + ^{13}CO reaction on Pd(110). No $^{15}N_2$ signal at the surface normal. (b-d) Angular distributions of desorbing $^{15}N_2$ in the plane along the [001] direction at different temperatures. (e) The distribution at 750 K is from the reaction of $^{15}N_2O + D_2$. (Ref. 52)

Fig. 8 ^{15}NO reduction on Rh(100); Surface temperature dependence of AR-$^{15}N_2$ signals at the surface normal and 70° off normal toward the [001] direction in a steady-state $^{15}NO + D_2$ reaction. The latter signals were normalized to the surface area for measurements in the surface-normal direction. The signals observed in the direction of the increasing surface temperature are designated by closed symbols, and those in the downward direction, by open symbols. The data in the range of 400-800 K were expanded in the inset. The angular

distributions of desorbing $^{15}N_2$ at T_S = 664 K, 760 K, and 720 K are shown on the right column. A typical deconvolution is shown by broken curves. (Ref. 53)

Fig. 9 Infrared emission spectra from the product CO_2 in CO oxidation on Pd(111) observed at the surface normal (a) and 30° off normal (b) directions. The total pressure in front of the surface is 0.49 Pa. The CO/O_2 flux ratio is 2:1, and the surface temperature is 700 K. The angle resolution is 16°. Fine lines show the observed spectra with a wave number resolution of 4 cm^{-1}. Thick solid lines show the optimum simulated results. The vibrational (T_{vib}) and rotational (T_{rot}) temperatures used for simulations are listed. For comparison, the best fits at 0° are drawn by the broken lines in the spectrum at 30°. (c) Angle dependence of the rotational and vibrational temperatures. (d) An energy partitioning model. (Ref. 9)

Fig. 10 Characters in repulsive CO_2 desorption from the CO(a) + O(a) associative process. (a) Side views of non-reconstructed fcc(110) (1×1) and reconstructed fcc(110) (1×2) planes. A long-bridge site in the trough on the (1×1) form works as the adsorption site for O(a) and emits CO_2 along the surface normal. On the (1×2) form, a three-fold hollow site on the declining terrace is suitable for O(a) adsorption and emits CO_2 into the inclined direction. The dashed-line ellipses indicate the size of the CO_2 molecule drawn using the van der Waals radii. (b) Typical

spatial distributions showing the symmetry and orientation of the reactive desorption site on Pd(110) (1×1) and Pt(110) (1×2). (Ref. 21)

Fig. 11 Surface phase diagram deduced from the angular distributions of desorbing CO_2; Logarithms of CO pressure (P_{CO}) at the kinetic transition (open symbols) and site-switching (closed symbols) at two fixed oxygen pressures are plotted against the reciprocal of surface temperature (T_S) and three-dimensional graphs representing spatial distribution in each region (Ref. 80)

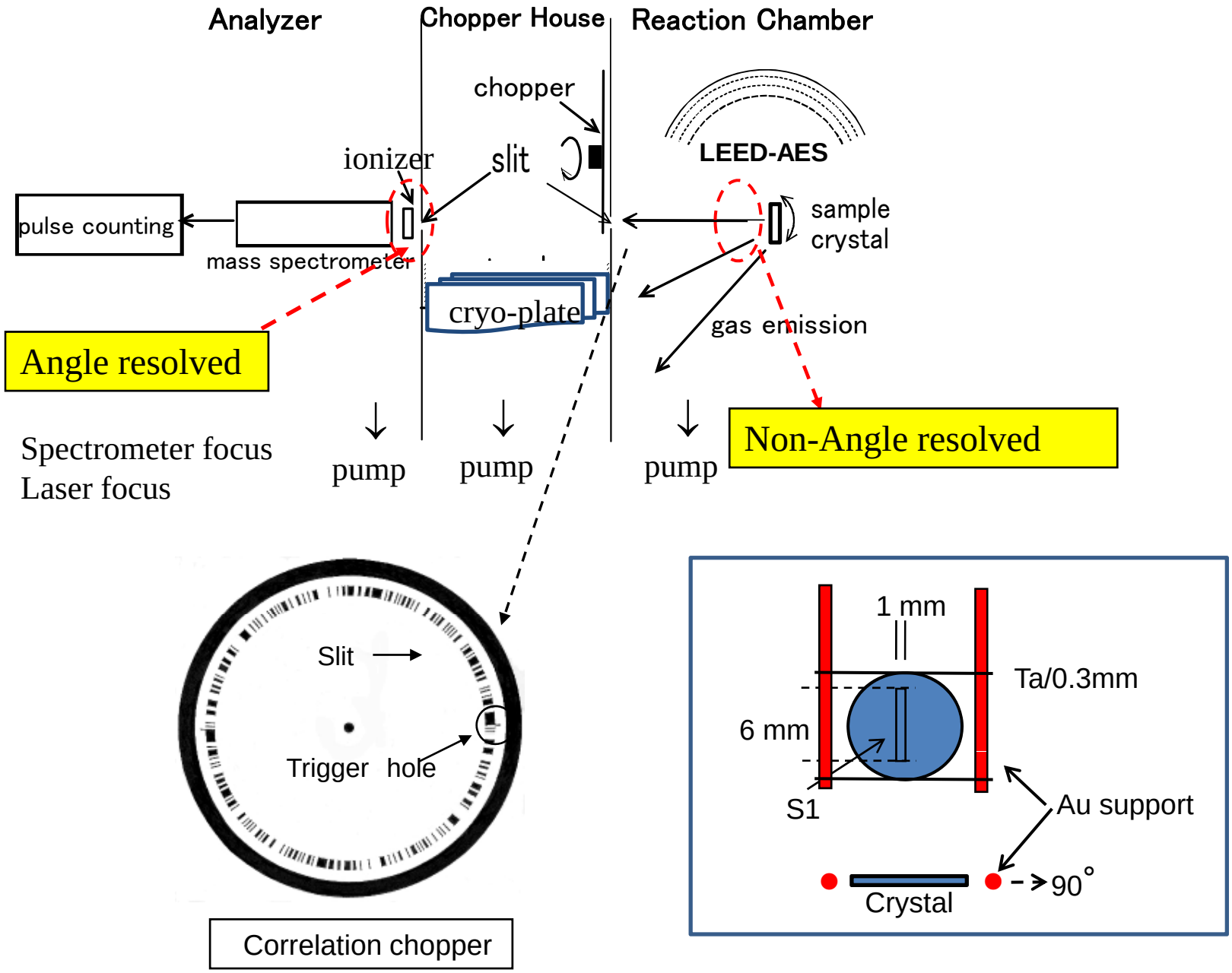

Fig.1 Matsushima

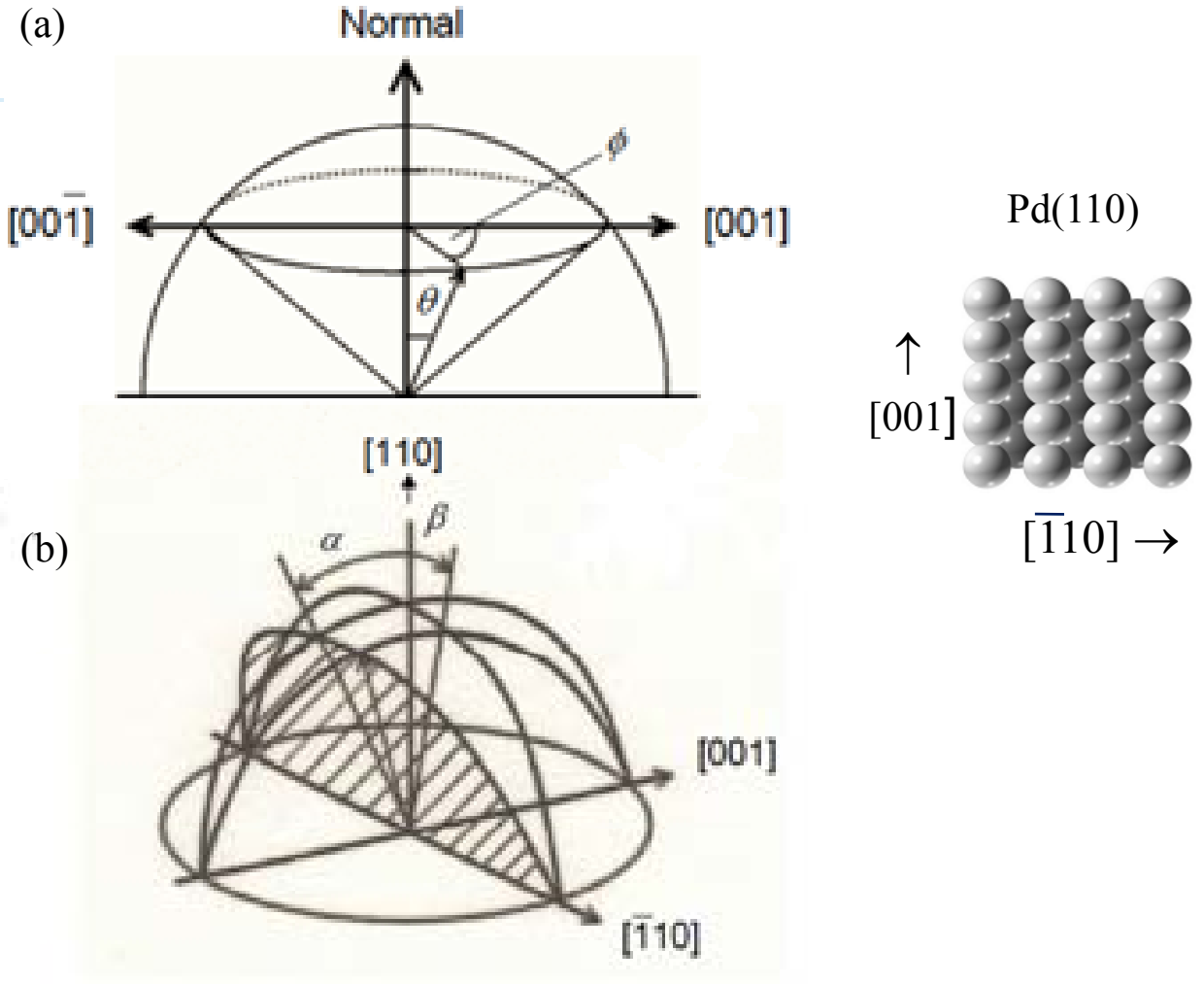

Fig.2 Matsushima

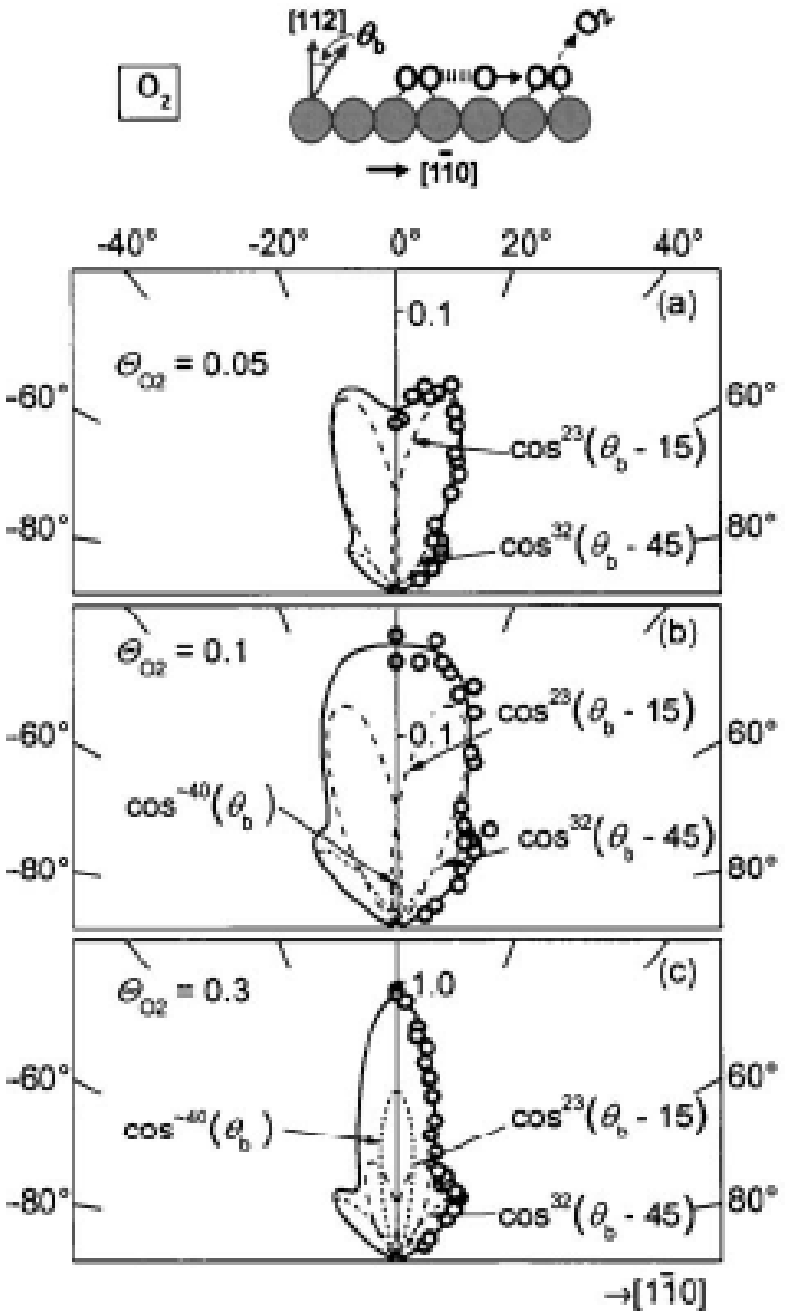

Fig. 3 Matsushima

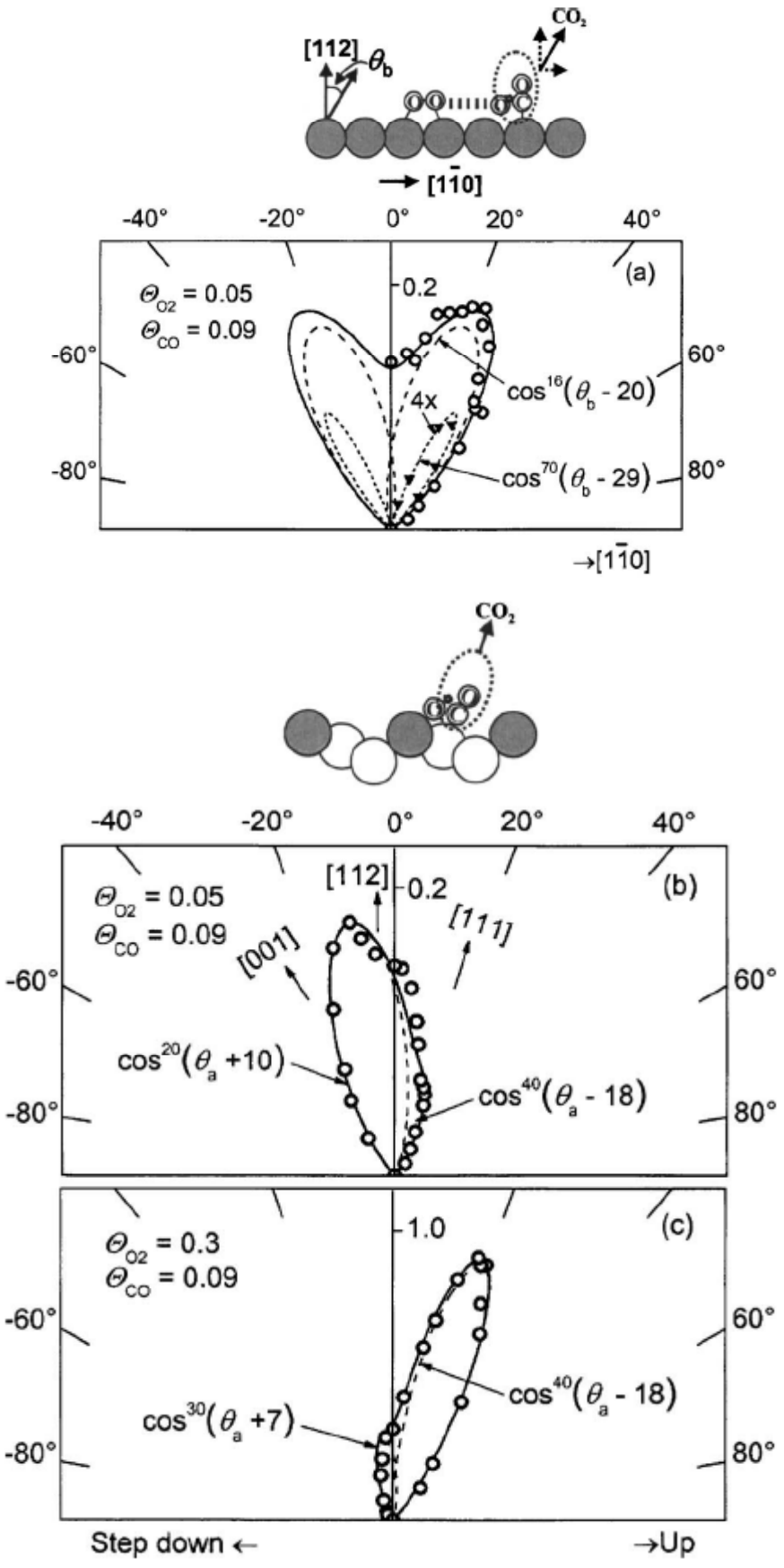

Fig. 4 Matsushima

$N_2O(a) \rightarrow N_2(g) + O(a)$ / Rh(110)

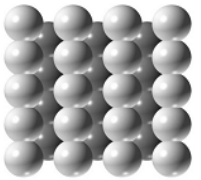

→ [001]

Enhanced by O(a) in a small amount

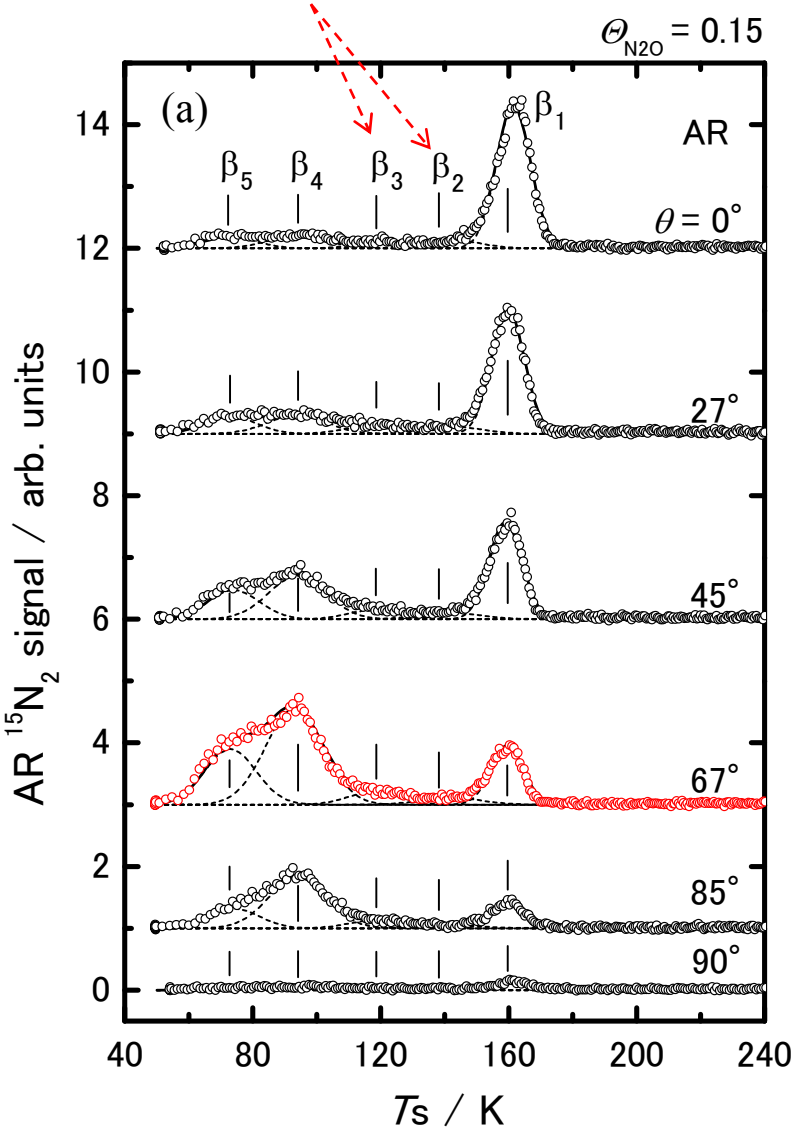

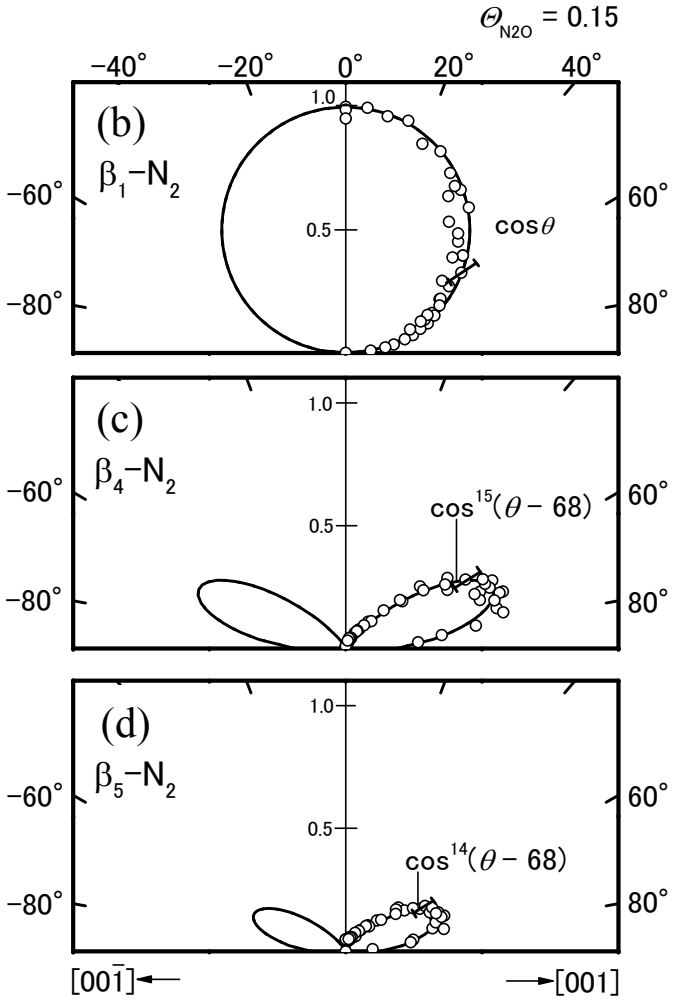

Fig.5 Matsushima

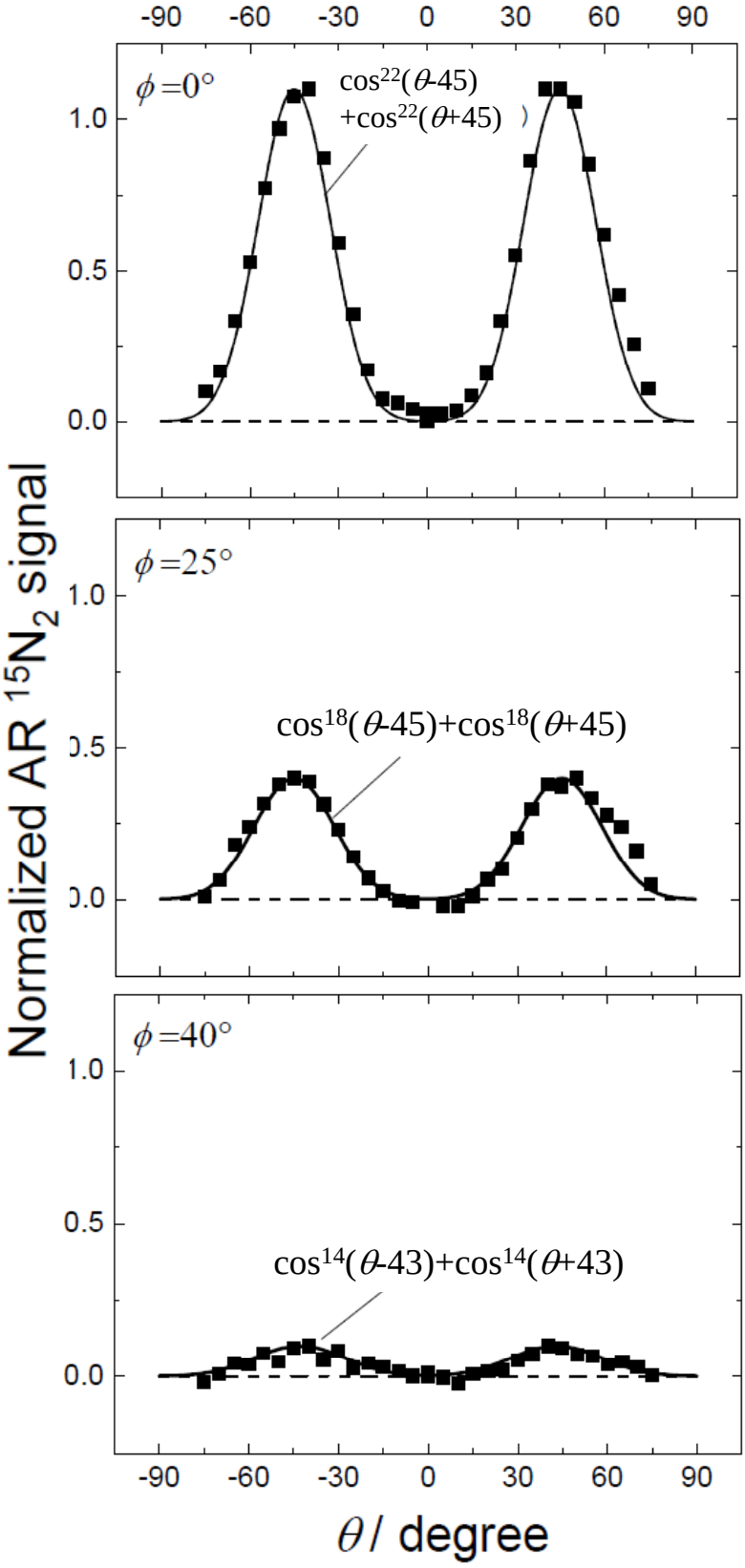

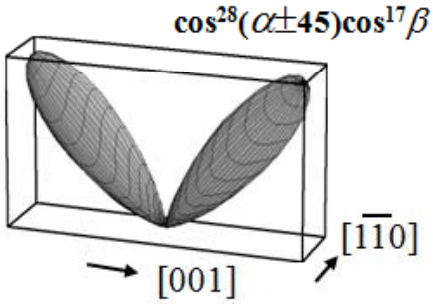

Fg. 6 Matsushima

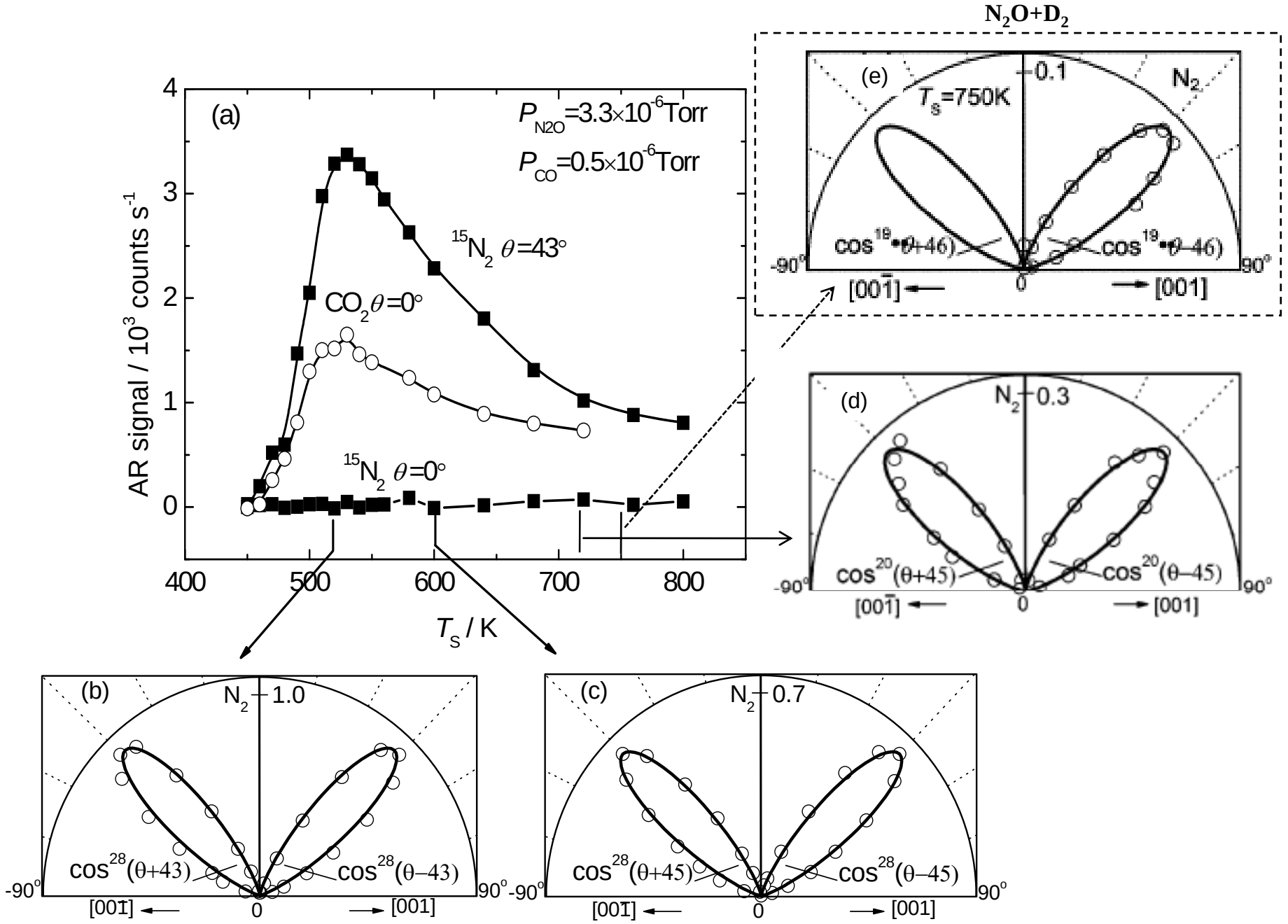

Fig.7 Matsushima

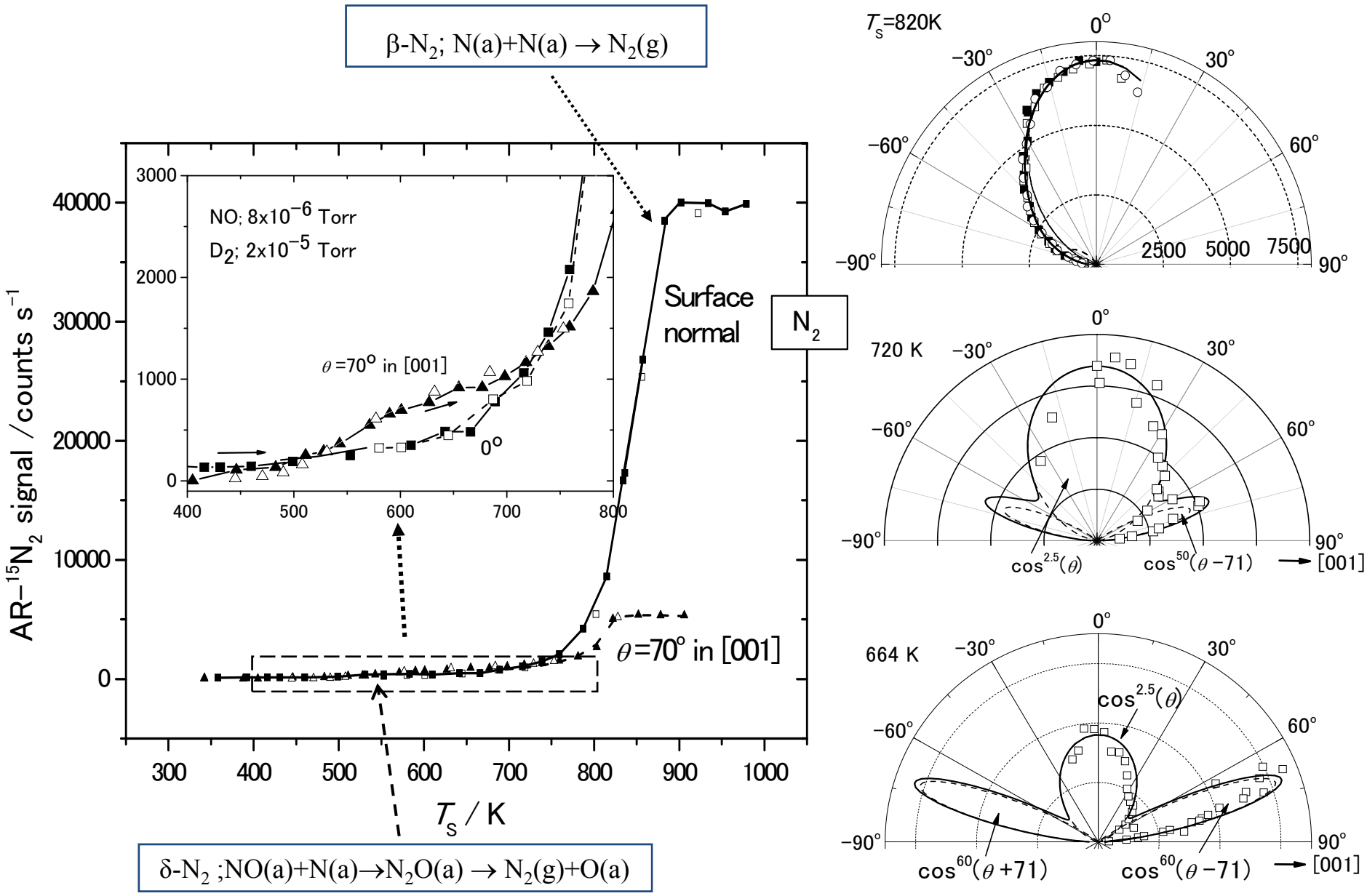

Fig. 8 Matsushima

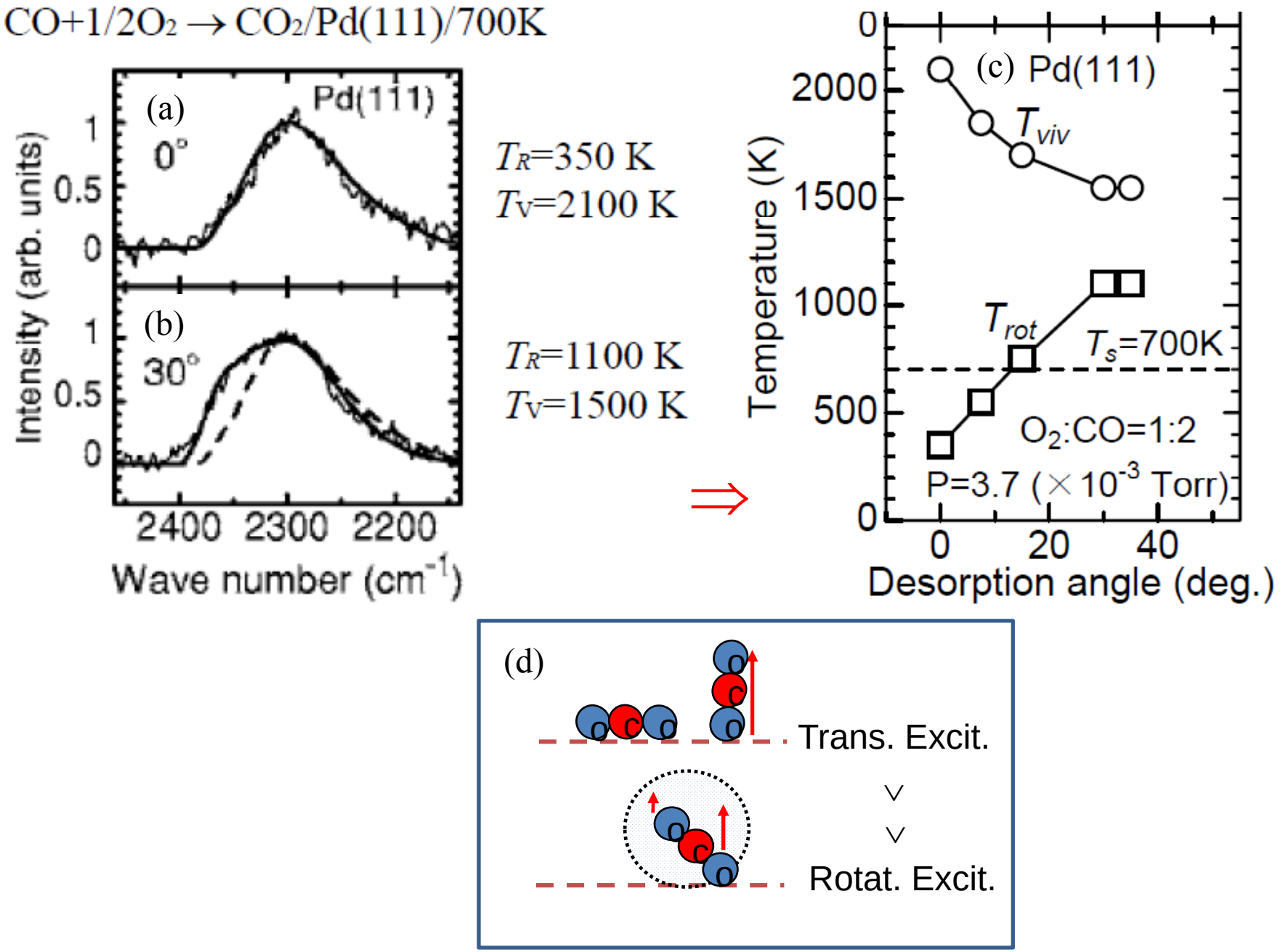

Fig.9 Matsushima

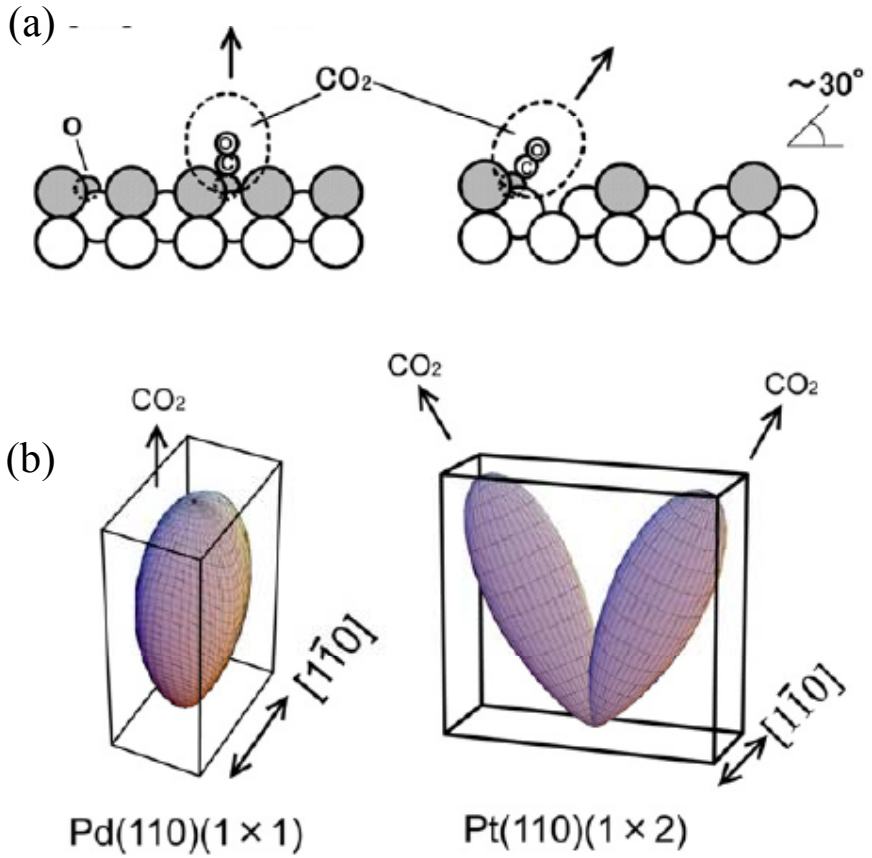

Fig. 10 Matsushima

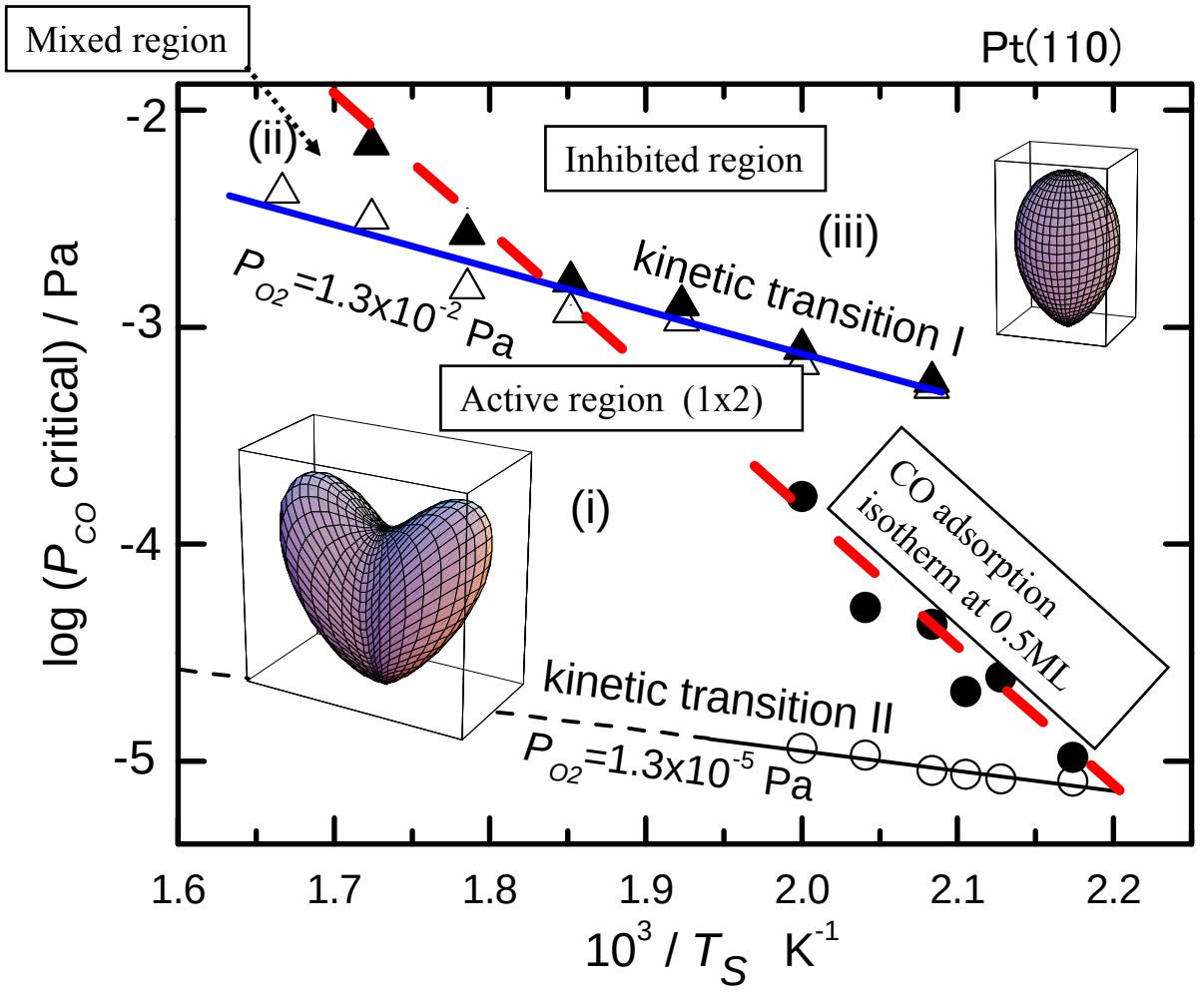

Fig.11 Matsushima